

1 Terminator Double Layer Explorer (TerDLE): Examining the Near-Moon Lunar  
2 Wake

3  
4 W. M. Farrell<sup>1</sup>, P. E. Clark<sup>2</sup>, M. R. Collier<sup>1</sup>, B. Malphrus<sup>3</sup>, D. C. Folta<sup>1</sup>, M. Keidar<sup>4</sup>, D. C.  
5 Bradley<sup>1</sup>, R. J. MacDowall<sup>1</sup>, J. W. Keller<sup>1</sup>

6  
7 1. NASA/Goddard Space Flight Center, Greenbelt, MD

8 2. NASA/Jet Propulsion Laboratory, Pasadena, CA

9 3. Morehead St. University, Morehead, KY

10 4. George Washington University, Washington, DC

11 012121

12  
13 Abstract: As the solar wind flows by the Moon, an anti-sunward directed low-density wake  
14 forms as the plasma expands to fill-in the trailing void in the plasma flow. Analytical modeling  
15 and modern plasma simulations suggest that plasma quasi-neutrality could possibly be broken  
16 close to the terminator obstruction as solar wind electrons expand into the wake ahead of the ions,  
17 leading to the formation of a standing (time-stationary) double layer. The objective of the  
18 Terminator Double Layer Explorer (TerDLE) is to extend the fundamental understanding of the  
19 plasma expansion into the trailing near-vacuum wake region by (1) identifying any plasma  
20 expansion density anomalies at low altitudes near the terminator wake initiation region, (2)  
21 assessing the highly variable solar wind's effect on low-altitude wake region, and (3) determining  
22 if plasma neutrality is maintained or lost during passages through the low altitude expansion  
23 region. The mission concept uses a propulsion-driven cubesat with ion spectrometer and plasma  
24 wave system in elliptical orbit about the Moon with periselene near the terminator. Over the course  
25 of the mission, the periselene decreases, placing the cubesat ever-closer to the terminator wake  
26 initiation location – and the possible non-neutral region.

## 1. Introduction

The Moon is an obstacle to the outward flowing solar wind plasma, and a substantial plasma perturbation trails the body to over 17000 km (or 10 lunar radii,  $R_L$ ) downstream (Farrell et al., 1998, 2002). The conventional wisdom was that the Moon absorbs near 100% of the incident solar wind on the dayside, thereby leaving a trailing plasma void - almost a near perfect vacuum - in its wake. Early exploration of the lunar space environment by spacecraft like Explorer-35 and Apollo sub-satellites focused on the unexpected and complicated magnetic signature in the trailing wake region (Ness et al., 1968; Ness and Schatten, 1969; Ness, 1972; Schubert and Lichtenstein, 1974). The plasma-vacuum interface (i.e., the wake flank) was described as an extended magnetohydrodynamic tangential discontinuity which disallowed solar wind ion inflow in regions anti-sunward of the Moon (Spreiter et al., 1970).

Serendipitously, a new view of the lunar wake resulted when the Wind spacecraft made transits at a few lunar radii downstream (for trajectory maneuvers). During these passages, the wake was investigated with modern plasma ion and electron spectrometers (Ogilvie et al. 1996; Bosque et al, 1996), magnetometers (Owens et al., 1996, Farrell et al., 1996) and plasma wave system (Bale et al., 1997, Farrell et al., 1997). The observations were extraordinary: that the ions do indeed expand into the trailing wake region via a plasma expansion process like that found to occur at space shuttle (Tribble et al., 1988, 1989).

Specifically, at the plasma-vacuum interface, energetic electrons are thought to propagate into the void ahead of the more massive ions, and in doing so create an expansion E-field that deflects the ion flow into the void. The ions become accelerated by this E-field to form ion beams (Samir et al., 1983, Ogilvie et al., 1996). For a magnetic field line crossing the cylindrical wake structure, counter-streaming ion beams are launched from the edges of the void; these flowing toward the central wake region along the threading magnetic field lines (Ogilvie et al., Clack et al., 2004; Halekas et al., 2011). These counter streaming ion flows were also found to be the source of intense ion-ion plasma wave activity (Farrell et al., 1997, 1998).

In the late 1990s/early 2000s, the Lunar Prospector (LP) spacecraft made over 6000 passes through the wake region from 115 km to as low as 20 km altitude. Halekas et al (2005) showed that the observations, both as an ensemble and in individual passes, were consistent with a plasma expansion of a kappa distribution of electrons flowing into the trailing void. Unfortunately, there

67 were no corresponding ion observations, and the lack of ion observations of the expansion is a  
68 reason to revisit this near-Moon region with TerDLE.

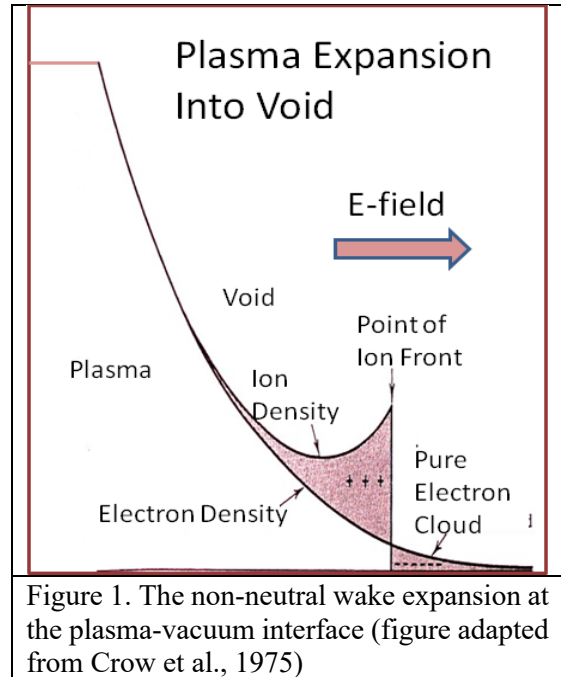
69 In the late 2000s, plasma instrumentation onboard Japan's Kaguya spacecraft also observed  
70 the plasma expansion, but also reported on a 'Type II wake' that was found in about 5-10% of  
71 near-Moon wake crossings (Nishino et al., 2010). Specifically, dayside reflected solar wind  
72 protons (Saito et al., 2008) could perform a circular trajectory about the local magnetic field taking  
73 these ions directly into the trailing wake. In doing so, a proton-governed region (PGR) is formed  
74 that creates an E-field that accelerates electrons into the wake. In this case, near the PGR, the E  
75 field is directed opposite to the normal expansion process, and causes the near-Moon electrons to  
76 accelerate into the void.

77 The twin THEMIS-ARTEMIS spacecraft are currently in orbit about the Moon making  
78 key measurements of pickup ions (Halekas et al., 2012), unusual wake geometries (for example,  
79 Poppe et al., 2014) and the overall wake structure (Zhang et al., 2014; Halekas et al., 2014; Zhang  
80 et al., 2016; Xu et al., 2019). One spacecraft is traveling prograde, and the other retrograde, about  
81 the Moon and both are in ~100 km by 19000 km low inclination orbits (Angelopoulos et al., 2010).  
82 Both THEMIS-ARTEMIS spacecraft have an ion spectrometer, electron spectrometer, and plasma  
83 wave system (McFadden et al., 2008; Bonnell et al., 2008). The local time of periselene will vary  
84 and only occasionally will it occur just nightside of the terminator. To date, there have been no  
85 systematic THEMIS-ARTEMIS studies of the near-Moon wake flank – the wake initiation region  
86 - just downstream of the terminator, especially examining a large set of passes just nightside of  
87 the terminator.

88 We thus describe herein a cubesat concept called TerDLE that explores the lunar wake  
89 region at very low altitudes – in regions just downstream of the terminator obstacle – to examine  
90 the early evolution of the plasma flow into the trailing void. TerDLE will also search for a non-  
91 neutral region called a double layer (i.e., adjacent oppositely charged plasma regions) that might  
92 form immediately downstream of the terminator. Section 2 further describes the expected near-  
93 Moon plasma discontinuity at the terminator. Section 3 provides the TerDLE mission objectives  
94 and Section 4 provides a brief description of the TerDLE instruments. Section 5 describes the  
95 TerDLE implementation as a 12 kg/6U cubesat while Section

96 6 describes enhancements to the mission, including other instruments, that could be accommodated  
97 on a larger  
98 bus to enhance the science.

99 We note that TerDLE was submitted as a  
100 proposal to the 2014 NASA/Heliophysics  
101 Technology and Instrument Development for  
102 Science (H-TIDeS) solicitation and, as a payload,  
103 was required to fit in a 12 kg, 6U cubesat bus to be a  
104 carried as a deployable package onboard Artemis-1.  
105 We thus describe the mission concept in this limited  
106 context in Section 5 – but fully realize that a larger  
107 spacecraft with added complementary instruments  
108 could also target this same objective. Thus, alternate  
109 scenarios for a larger system will be described in  
110 Section 6.



## 112 2. The Near-Moon Plasma-Vacuum Discontinuity

113  
114 Consider the development of a time-stationary near-perfect plasma-vacuum discontinuity  
115 like that which would form just downstream of the lunar terminator. It would be limited in  
116 downstream extent but should form an annulus about the entire terminator.

117 The plasma expansion in this initiation region should be a near-perfect discontinuity.  
118 However, there are two different views of the early expansion period, depending upon the initial  
119 assumptions: Analytical formalism appears in the literature that solves the fluid equations by  
120 initially setting the electron and ion density to be equal (quasi-neutrality; see review by Samir et  
121 al. (1983). Applications using hybrid plasma simulations also fix plasma neutrality (the ion  
122 densities equal the electron densities,  $n_i = n_e$ ). In doing so, the ions expand into the void in  
123 concentrations identical to the electrons.

124 However, Crow et al., (1975) also used the fluid equations to derived the expansion process  
125 but relaxed the assumption of neutrality in their analytical formalism. **Figure 1** illustrates their  
126 results: That the electrons migrate into the void ahead of the ions, creating an ‘electron cloud’

127 region that forms the negative polarity region of a double layer. These electrons are actually the  
 128 fastest electrons in the solar wind energy distribution (i.e., high energy tail) . Further, because of  
 129 the E-field, the ions are accelerated into the void to form an ion beam. This process creates an ‘ion  
 130 front’ that consists of the fastest group of ions in the expansion. The result of Crow et al.’s  
 131 analytical approach suggests that a standing double layer – a region where the normally charge-  
 132 neutral plasma is separated into opposite polarities (predominantly ions spatially adjacent to  
 133 predominantly electron) - should form at the earliest

134 times in the plasma expansion  
 135 process.

136 Double layers are of general  
 137 interest in plasma physics, since they  
 138 represent regions that are not in charge  
 139 equilibrium and possessing a large cross-  
 140 layer E-field, and thus an electrical  
 141 potential drop that is capable of  
 142 accelerating ions and electrons. For  
 143 example, double layers have been found  
 144 in Earth’s auroral regions creating  
 145 electron and ion acceleration in the  
 146 region (Ergun et al., 2004). The idea that  
 147 the Moon also possesses such a particle  
 148 acceleration region is intriguing and

149 affirms that view that the plasma environment disrupted by the Moon is a new form of a plasma  
 150 physics laboratory to examine basic plasma processes.

151 In order to test whether neutrality is maintained in the wake expansion process, as described  
 152 by Crow et al. (1975), a series of particle-in-cell kinetic simulations were run modeling the wake  
 153 region near its obstruction along the terminator (Farrell et al, 2008). These particle-in-cell codes  
 154 do not set  $n_i = n_e$ , but allow the ion and electron populations to evolve and be controlled by the  
 155 electric field that forms in the spatial separation. The interplanetary magnetic field (IMF) in the  
 156 solar wind in these simulations is assumed to be quasi-perpendicular to the wake flank. As shown  
 157 in **Figure 2**, a void in the simulated solar wind plasma is created and the plasma is allowed to

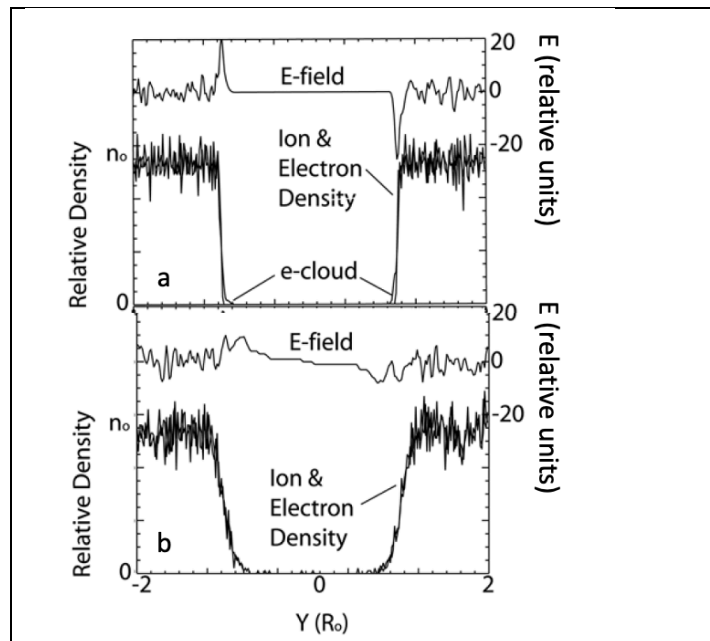


Figure 2: PIC simulation of the plasma expansion E-field behind the Moon for (a) early times in the simulation and (b) later times in the simulation (adapted from Farrell et al, 2008).

158 expand into the void along the Y direction (same direction as the IMF). As predicted by Crow et  
159 al. (1975), at early times in the simulation (Figure 2a), the electrons move into the void ahead of  
160 the ions to form an electron cloud (labeled 'e-cloud' in the figure). The E field also has its largest  
161 value at the electron cloud interface. At later times in the simulation (Figure 2b), the ions have  
162 caught up with the electrons. Note that while the simulation is a one-dimensional model of the  
163 expansion, the cross-wake profile at each increasing time steps represents a position further  
164 downstream from the Moon since the Y-density profile convects downstream at the solar wind  
165 speed,  $V_{sw}$ . The results suggest that there should be a separation of electrons from ions at the  
166 plasma-vacuum interface located immediately downstream of the terminator obstruction point.  
167 Most likely this layer changes morphology with prevailing IMF direction and solar wind  
168 conditions, and such changes will also be investigated by TerDLE.

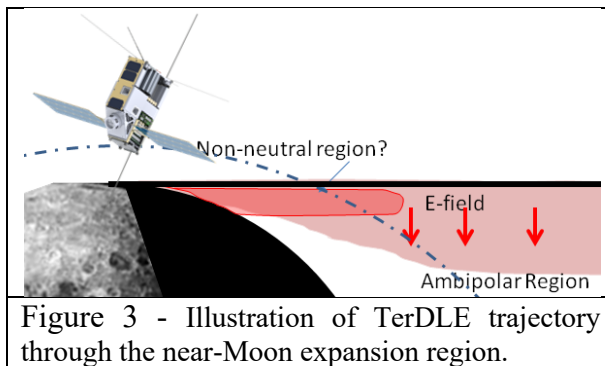
169         Regarding the size of the non-neutral region, two-dimensional particle-in-cell simulations  
170 of the plasma expansion suggests the presence of an extended region. Specifically, Nakagawa  
171 (2013)'s simulation found that a non-neutral region forms behind the Moon, having an ion front  
172 ( $n_i > n_e$ ) protruding  $\sim 0.2 R_l$  inward from the wake at a downstream distance of near  $1 R_l$ . The  
173 modeled region is substantially larger than the solar wind Debye length (of  $\sim 15$  m). The finding  
174 of an extended non-neutral region is similar that derived in the modified one-dimensional  
175 simulations of Farrell et al. (1998, 2008). However, if such an extended non-neutral region existed  
176 in downstream regions, it should have been observed and reported by THEMIS-ARTEMIS. While  
177 Crow et al. (1975) modeled a non-flowing ion and electron expansion (fluid not convecting  
178 downstream), their results can be used to predict the extent of the non-neutral region in its initial  
179 stages. Specifically, in Figure 9 of Crow et al. (1975), it is surmised the non-neutral region near its  
180 initiation has a width of  $> 100$  Debye length (1.5 km) and can propagate downstream at least 50  
181 ion plasma periods ( $> 7$  km downstream for a 400 km/s solar wind convection speed). Such a non-  
182 neutral region would be at the limit of TerDLE detection, requiring fast sampling at the end of the  
183 TerDLE mission. In this more limited case, TerDLE might not detect the non-neutral region, but  
184 place a well-defined limit on its spatial size.

185         Two-dimensional particle-in-cell simulations of plasma expansion into regional  
186 obstructions, like polar craters, etc., also show the formation of the double layer immediately  
187 downstream of the obstruction (Zimmerman et al., 2011, 2012, 2013). These ion sonic wakes and  
188 local expansion regions are considered 'self-similar' structures (Samir et al., 1983) with the

189 regional mini-expansions being representative of the larger expansion at a global level.  
190 Zimmerman et al. (2013) demonstrated analytically and via simulation that a set of recursive  
191 regional wakes created by local topography over the terminator merge to form a larger singular  
192 and homogenous wake as the downstream distance progressively increases.

193 TerDLE specifically targets the plasma-vacuum interface downstream of the terminator to  
194 map out electron and ion morphology, to  
195 examine external controlling influences on the  
196 plasma expansion process and to search for and  
197 identify the possible electron cloud/double layer  
198 regions, if they are present at TerDLE's altitude.

199 **Figure 3** illustrates TerDLE's passages through  
200 the heart of the plasma expansion region.



201

202

### 203 3. Objectives, Significance, and Closure

204

205 The plasma expansion region in the near-Moon environment is just beginning to be appreciated  
206 as its own unique plasma physics laboratory. Consequently, this special plasma region makes an  
207 ideal target for a lunar Cubesat mission. The TerDLE science objectives are:

#### 208 1) Identify any plasma expansion density anomalies at low altitudes near the terminator.

209 In the outer wake regions, spacecraft like Wind and THEMIS-ARTEMIS have demonstrated that  
210 the plasma expansion process fits nicely to kinetic simulations of an ion sonic expansion. For  
211 example, Xu et al. (2019) mapped out the lunar wake potential out to 4  $R_L$  using over 6.5 years of  
212 THEMIS-ARTEMIS data and the observations were comparable to a plasma expansion model.  
213 However, simulations suggest that the plasma discontinuity region immediately downstream of  
214 the terminator/obstruction has a very complex density structure, possible even a break in neutrality.  
215 The early expansion region may also contain anomalous plasma density fluctuations/plasma waves  
216 that have not been observed previously that form at the edges of the flank due to currents associated  
217 with the expansion process. Thus, an examination of this region at very low altitudes should be  
218 revealing.

219       **2) Assess the solar wind’s effect on the presence and structure of the wake flank region.**

220       The solar wind density, temperature and magnetic field strength & orientation are all variable in  
221       the solar wind – changing on time scales of minutes. The Moon and wake may even undergo  
222       changes associated with a passing coronal mass ejection or other extreme space weather event.  
223       The Type II wakes (Nishino et al., 2010) also represent exceptions to the nominal expansion  
224       process. Hence, understanding the nature and structure of the near-Moon expansion region as a  
225       function of driving external conditions will further our understanding of the expansion process  
226       itself. By its ever-changing nature, the driving solar wind provides opportunities to advance our  
227       understanding of the expansion process (i.e., for slow and fast speeds, warm and cold plasma  
228       temperatures, varying IMF conditions, etc.). Upstream monitors like Wind and ACE, along with  
229       local monitors THEMIS-ARTEMIS will all provide critical information on external environmental  
230       conditions.

231       **3) Determine if plasma neutrality is maintained or lost during passages through the**

232       **expansion region.** Modeling suggests the plasma does not maintain neutrality at the wake flank  
233       close to the Moon. The size and extent of this non-neutral region remains unknown and a  
234       systematic search for and identification of non-neutral plasma layers has yet to be made. Xu et al.  
235       (2019) did report on THEMIS-ARTEMIS passes close to the Moon, presenting statistical analysis  
236       from many passes of the electrostatic potential in the near-Moon region. The resolution of the  
237       averaging interval closest to the Moon was  $\sim 0.1$  lunar radii and the potential alone cannot indicate  
238       if neutrality is lost since the potential still varies smoothly across the boundary (see Figure 3 of  
239       Crow et al., 1975). TerDLE’s instrument complement and unique orbit will allow a search at very  
240       low altitudes examining explicitly the differences in  $n_e$  and  $n_i$  to derive loss of neutrality. It should  
241       be noted that this search for the double layer is a primary objective. Also note that the failure to  
242       find the double layer does not mean mission failure – instead TerDLE then provides an upper  
243       limit/constraint on the angular width and downstream extent of the double layer. Thus, even a non-  
244       detection has value in providing the spatial constraints of the non-neutral region.

245

246

Science Objective	Measurement Requirements	Mission Requirements	Instrument Requirements	Science Closure
Identify any plasma expansion density anomalies at low altitudes near the terminator	Measure $n_e$ & $n_i$ from 0.0001 (wake) to 100 per cc; Measure during terminator crossings (LT 6 Hr and 18 Hr +/- 0.5 Hr; Measure close to Moon (< 50 km))	-Periselene at low altitudes in vicinity of terminator obstruction point  -Orbit to have progressively reducing perislene to below 100 km	- $n_i$ : 10 to 0.01/cc, 20-5000 eV -VLF E: 0.01-100 kHz ; > 0.01 mV/m providing $n_e$ from < 0.001/cc to 123/cc -Sampling on 1 sec time scales	Obtain $n_i$ , $n_e$ , and plasma waves and observe plasma-vacuum discontinuity morphology as obstruction point is approached
Assess the solar wind's effect on the presence and structure of the Near-Moon expansion region	Correlate expansion characteristics and with prevailing IMF and solar wind conditions	-Point directly into solar wind flow once per ~10 sec interval  -Multiple crossings for months with varying SW conditions	- $n_i$ : 10 to 0.01/cc, 20-5000 eV -VLF E: 0.01-100 kHz ; > 0.01 mV/m providing $n_e$ from < 0.001/cc to 123/cc  -THEMIS-ARTEMIS or upstream monitors to get SW and IMF	Derive plasma expansion process under varying external IMF and SW conditions. Determine if there are periods when DL disappears. Observe other unusual wake types (like Type II wakes reported by Kaguya)
Determine if plasma neutrality is lost during passages through the ambipolar region	Create $n_i$ - $n_e$ and $dn_e/dx$ , $dn_i/dx$ profiles to determine if there are consistent differences between these profiles.	-No predefined inclination required	- $n_i$ : 10 to 0.01/cc, 20-5000 eV -VLF E: 0.01-100 kHz; > 0.01 mV/m providing $n_e$ from < 0.001/cc to 123/cc	Compare profiles of $n_e$ and $n_i$ to determine if Crow's electron cloud and ion front are observable. Close this fundamental issue out.

247

248 Table 1: The TerDLE Science Traceability Matrix (STM)

249

250 **Table 1** is the TerDLE science traceability flowdown from science objectives to mission  
251 and instrument requirements through to science closure. The methodology for determining the  
252 electron cloud/double layer is simple: to compare the measured electron-to-ion density difference  
253  $n_e - n_i$  and also the variations in the slope of the densities  $dn_e/dx$  and  $dn_i/dx$  (which removes relative  
254 offsets).

255 Mission requirements include moving from a high speed hyperbolic orbit imparted at  
256 cubesat ejection into a captured elliptical lunar orbit with a decreasing periselene at the terminator;  
257 this in order to map out the structure of the Near-Moon expansion regions. By the nature of the  
258 orbit design, TerDLE will be on orbit for months and will obtain a large statistical set (> 100) wake  
259 flank crossings under varying solar wind conditions. The wake flank region is a relatively easy  
260 target for study since it is fixed in local time and will be transited twice per orbit by TerDLE.

261 In examining the measurement requirements in Table 1, one could easily assume an ideal  
262 sensor for directly measuring plasma densities is a Langmuir probe, which has had great success  
263 operating in the dense Enceladus plasma torus and Titan ionosphere. However, such probes lose  
264 sensitivity in low densities (below about  $10/\text{cm}^3$ ) since they cannot collect enough plasma current  
265 at the sensor head to detect the low densities and flux levels expected in the lunar plasma wake,  
266 near  $0.01/\text{cm}^3$ . Consequently, we build an ‘effective’ Langmuir probe using a set of  
267 complementary sensors: An ion spectrometer (IS) to obtain  $n_i$ , and a plasma wave system (PWS)  
268 operating from 0.01 Hz to 100 kHz to measure VLF E-fields and measure  $n_e$  from the intense  
269 emission at the electron plasma frequency,  $f_{pe}$ . While an electron spectrometer would obtain the  
270 energy character of the electrons, such instruments are highly susceptible to negative spacecraft  
271 charging like that expected in the shadowed wake - which then could potentially create an under-  
272 calculation of the  $n_e$  moment. In contrast, the observation of the electron plasma frequency  $f_{pe}$   
273 emission allows for a direct, high resolution measurement of  $n_e$ .

274 TerDLE IS and PWS can provide an accurate measure of  $n_e$  and  $n_i$ , enabling a systematic  
275 study of the region downstream of the obstructed flow. The gradient in density,  $dn_e/dx$  and  $dn_i/dx$ ,  
276 can also be derived which may even be more robust against any systematic offsets in the direct  
277 measurement of the density (although possibly adds noise depending upon fluctuations in the  
278 values). Besides the  $f_{pe}$  emission, other plasma waves could also be detected at and near the  
279 boundary crossing, like broadband electrostatic noise (Farrell et al., 1997). Using  $n_e$ ,  $n_i$ ,  $dn_e/dx$ ,  
280  $dn_i/dx$ , and plasma waves, investigators can examine the character of the wake formation region  
281 near the obstacle location and determine if neutrality is lost. This data analysis approach  
282 specifically addresses the closure of the first and last science objectives in the Traceability Matrix  
283 in Table 1.

284 External conditions will alter the nature of the expansion and data monitors like ACE,  
285 WIND, and THEMIS-ARTEMIS can be used to correlate the morphology of the expansion with  
286 driving conditions. Investigators can then correlate the key TerDLE parameters with prevailing  
287 space environmental conditions to determine if a systematic effect is observed. Correlations of  
288 wake  $n_e$ ,  $n_i$ ,  $dn_e/dx$ ,  $dn_i/dx$  and plasma waves as a function of driving solar wind and IMF can be  
289 made. This data analysis approach specifically addresses the closure of the second science  
290 objectives in the Traceability Matrix in Table 1.

291

#### 4. TerDLE Instrumentation

Since the cubesat has limited payload carrying capability, only two instruments were chosen to be onboard - the IS and PWS. Both systems were expected to be built at NASA-Goddard Space Flight Center. The IS heritage is drawn in part from the flight-proven FASTSAT and VISIONS MINI-ME neutral atom spectrometer (Rowland et al., 2011; Collier et al., 2015). Figure 8 and 9 of Rowland et al. (2011) displays the MINI-ME energetic neutral system, with the system following the conversion surface to be used as the TerDLE ion detection system (with a reverse in polarity). For TerDLE applications, the head of the ion instrument that samples the local plasma environment consists of deflectors and two nested toroids. A microchannel plate (MCP) stack detects ions that have the correct energy to transverse the gap between the toroids based on the applied stepped voltage between the toroids. The TerDLE/IS and all associated electronics was to fit within a 1U segment of the 6U CubeSat. The IS energy range covers 20-5000 eV, and its field-of-view about the central observing plane was expected to be 360° azimuthally and 10° latitudinally. However, added deflectors would then allow sampling of the ion distributions from about 30° to 45° above the central field-of-view plane, depending on ion energy.

The PWS was planned to be digital electric radio that operates from 0.01 Hz to 100 kHz. The radio consisted of a deployable antenna of ~ 1-m length which drives a VLF pre-amp. The pre-amp system is a slight modification of low-noise VLF amp built for the DSX search coils that have been in orbit in the radiation belts since mid-year 2019 (Scherbarth et al., 2009). The signal is digitized immediately behind this preamp and the remainder of the radio is a digital FPGA system that performs digital filtering and spectral analysis. The primary outputs are wave spectra that will allow a determination of the  $f_{pe}$  peak emission and thus the electron density. The  $f_{pe}$  emissions are stimulated by wake-created plasma instabilities (Bale et al., 1997).

#### 5. Mission Implementation as an Artemis-1 Cubesat

The original TerDLE concept was a 12 kg/6U cubesat was proposed to be deployed during the flight of the Artemis-1 mission. The TerDLE ion propulsion is low thrust ( $< 1$  mN) and thus the baseline transfer and lunar capture is very similar to the two-phase capture orbit of Lunar IceCube. Lunar IceCube is a selected mission to be deployed on the upcoming Artemis-1 flight.

323 The low thrust trajectory incorporates dynamical system (manifold) analysis similar to that used  
324 for the capture of the two THEMIS-ARTEMIS spacecraft. One such trajectory analysis  
325 representative of the transfer and capture process for Lunar IceCube is illustrated in Figure 7 of  
326 Clark et al. (2017). The TerDLE and Lunar IceCube have similar heritage (identical spacecraft  
327 builders, 6U/12kg cubesats, Artemis-1 payloads, similar orbit designs). We thus will reference  
328 Lunar IceCube in the TerDLE mission implementation herein since it is now manifested to fly on  
329 Artemis-1.

330 In Phase 1, TerDLE was initially to be injected into a hyperbolic orbit from the fast-moving  
331 Interim Cryogenic Propulsion Stage (ICPS) bus of Artemis-1. Direct injection into orbit about the  
332 Moon is not possible with the low thrust system. Instead, upon ICPS release, the cubesat would  
333 apply a modest thrust to target a lunar gravity assist that results in a ballistic transfer trajectory  
334 designed to encounter the Moon at a lower velocity. The post-lunar flyby energy would be reduced  
335 to that of a typical Sun-Earth/Moon system heteroclinic (Earth-Moon captured) manifold. TerDLE  
336 then would proceed in a long duration orbit including a series of Earth periapses to allow long-  
337 duration application of the thruster system. The combination of the orbit orientation, Earth  
338 periapsis, and the long-term thruster firings thus allows TerDLE to slow down for lunar capture  
339 (see Figure 7 of Clark et al. (2017) as an example of this capture). In effect, the thrust operations  
340 and the multibody dynamics are used to raise TerDLE's Earth orbit perigee to match a lunar orbit  
341 radius, adjust the timing of the lunar encounter, rotate the orbital line of apsides, and achieve a  
342 ballistic lunar encounter which reduces or eliminates lunar capture delta-V requirements. We note  
343 that each transfer and capture trajectory scenario is robust but highly unique to the specific launch  
344 date, Earth-Moon-Sun position, and release speed of the spacecraft. This transfer and capture phase  
345 is expected to take 50-100 days, depending upon the launch date and injection speed.

346 In Phase 2, now captured in a highly elliptical lunar orbit, TerDLE would use the low thrust  
347 system for many days each orbit to progressively reduce the aposelene. This phased thruster use  
348 places the spacecraft into its final science orbit having a periselene altitude well below one lunar  
349 radii. In the TerDLE orbit design, the thruster sequencing was such that the periselene would vary  
350 in altitude, with a periodically-occurring minimum periselene value that would progressively drop  
351 in altitude to values well below 100 km. Also, the elliptical orbit allows a comparison of the near-  
352 surface wake at periselene to that further downstream intercepted at aposelene. The orbit design  
353 was such that near the end of the mission, TerDLE would make a set of very low altitude periselene

354 passes at and just nightside of the terminator – locations just downstream of the wake initiation  
355 region.

356 The TerDLE cubesat for the Artemis-1 mission was planned to be built at Morehead State  
357 University (MSU), leveraging the team’s substantial and significant CubeSat system engineering  
358 and mission experience. The TerDLE development utilizes systems with significant LEO flight  
359 heritage and incorporates new nanosatellite technologies to develop an evolved, radiation-tolerant  
360 6U CubeSat bus designed to support interplanetary investigator science. The MSU 6-U deep space  
361 CubeSat possesses high power generation (for Lunar IceCube, 120 Watts of continuous power), a  
362 radiation-tolerant, distributed multiple processor-based payload processor system, a highly-  
363 capable miniaturized guidance/nav system designed for lunar missions, an innovative propulsion  
364 system, and a high through-put X-band communication system for lunar CubeSat missions.

365 The 6-U CubeSat Bus structure is based on a robust 2-wall structure matched to central  
366 mounting frames and capped by robust, milled bulkheads on the +Z and -Z faces. Subsystem  
367 enclosures and braces reinforce the structure throughout the length of the body, allowing the frame  
368 to hold very tight tolerances. The design also provides rigidity required to maintain integrity during  
369 vibration. The structure is simple to manufacture and assembles easily during test and integration.  
370 The open-sided concept provides easy access to subsystems for systems testing, improves thermal  
371 control, and is designed to meet NASA spacecraft venting standards. It serves as a chassis to  
372 accommodate four deployable solar panels, four deployable blade antennas, patch antennas, PWS  
373 antennas, a thermal management system and an electromechanical deployment system that stows  
374 and controls the deployments in compliance with the NASA launch system provider (LSP)  
375 secondary payload deployment restrictions. The structure has flight heritage and has consistently  
376 passed environmental testing (including vibrate and thermal-vacuum) at 3 dB above the NASA  
377 Goddard environmental standards.

378 The Morehead St. bus would integrate key components from expert partners. For Lunar  
379 IceCube, these partners include Blue Canyon Technology for the attitude control system, Pumpkin  
380 Inc. for custom solar panels, Busek for ion drive propulsion, JPL for the Iris x-band comm system.  
381 Like for Lunar IceCube, TerDLE was designed with multiple processors for redundancy. The  
382 C&DH architecture was intended to be distributed between the flight computer (Space Micro Proton  
383 Lite radiation tolerant processor, SMPL), avionics controller (XB1 C&DH), and the low-cost,  
384 radiation tolerant, high speed payload processor (Honeywell Dependable Microprocessor, HDM).

385 Each of the three processing systems would thus have capability to control basic spacecraft  
386 functions providing redundancy for risk mitigation.

387 Unlike Lunar IceCube, TerDLE was to utilize a Micro-Cathode Arc Thruster ( $\mu$ CAT)  
388 micro-propulsion subsystem that is an outgrowth of George Washington University (GWU)  
389 Micropropulsion and Nanotechnology Laboratory (MpNL) research in scalable small spacecraft  
390 electric propulsion. The system would provide  $> 600 \mu\text{N}$  of thrust and a total Delta-V  $> 870 \text{ m/s}$  -  
391 levels consistent with the low-energy baseline transfer and capture scenarios described above. The  
392 GWU team continues to successfully advance micro-thrust technology (see Zolotukhin et al.,  
393 2020).

394 The communication approach was to utilize a JPL Iris X-band transceiver coupled to broad-  
395 beam patch antennas and a Direct-to-Earth transmission to the high gain Morehead State 21-meter  
396 ground station, that is now an affiliated node on the NASA Deep Space Network (Deep Space  
397 Station 17). The proposed mission operations strategy will support a data throughput rate of a  
398 minimum of 128 kbs and ensure the acquisition of 16M Samples of data per day – more than  
399 enough to meet the science objectives.

400

## 401 **6. Discussion and Conclusions**

402

403 TerDLE was designed to target wake flanks that have electrons migrating into the void  
404 ahead of the ions – thereby creating an expansion E-field that is oriented to accelerate ions toward  
405 the center of the wake. However, there are other anomalous wake configurations that TerDLE can  
406 detect, like the proton-governed region discovered by the Kaguya spacecraft (Nishino et al., 2010).  
407 While the conventional wisdom used to be that 100% of the solar wind ions are absorbed on the  
408 lunar dayside, Kaguya and Chandrayaan-1 observations (Saito et al., 2008; Lue et al, 2011) suggest  
409 that anywhere from 1-50% of the incoming protons are reflected from the surface or near-surface  
410 magnetic anomalies. Further, these reflected protons maintain substantial energy upon reflection  
411 from the dayside magnetic anomalies ( $\sim 80\%$  of incoming energy). Some fraction of these dayside  
412 scattered ions will then undergo cyclotron motion in the IMF that carries their trajectories directly  
413 into the central lunar nightside/wake region to form a positive proton region called a ‘proton-  
414 governed region’ (Nishino et al., 2010; Xu et al., 2020). This anomalous clustering of positive  
415 protons in the central wake then accelerates electrons from the flanks into the wake in order to

416 maintain plasma neutrality. In this case, the expansion E-field is directed opposite to nominal  
417 orientation – with the E-field directed outward from the central wake region (see Figure 3 of  
418 Nishino et al., 2010; Figure 1 of Xu et al., 2020) in order to accelerate the electrons. This proton-  
419 dominated wake region was found in about 5-10% of lunar wake transits (Nishino et al., 2010).  
420 TerDLE will examine this region as well – at very low altitudes at the wake edge.

421         The initial TerDLE embodiment was a 6U/12 kg cubesat, which is a rather limited concept.  
422 However, the concept fit in a scope consistent with the solicitation (the ride and costs). The 2014  
423 HTIDeS proposal evaluation indicated there were four major strengths to TerDLE: (1) The topic of  
424 plasma expansion into a vacuum was a fundamental plasma process worthy of study, (2) the  
425 instruments selected could deliver the measurements needed to close Objective 1 and 2, (3) the  
426 proposal demonstrated a feasible mission and lunar orbit insertion scenario, and (4) the proposal  
427 demonstrated a mature cubesat bus. The two major weakness were similar in nature involving (1)  
428 a lack of description of instrument capabilities and (2) a lack of a description of the required  
429 instrument accuracy to uniquely identify the non-neutral region to thus close Objective 3. The  
430 concern was that the electron and ion density differences might be so subtle as to be  
431 indistinguishable as measured. As described above, kinetic simulations like that in Figure 2 and  
432 Nakagawa (2013) find that the non-neutral region just inward of the wake flank has a measurable  
433 density difference in an extended region that is detectable. However, analytical models of the  
434 expansion (Crow et al., 1975) suggest the region could be small in extent. At this point, the size  
435 and extent of a nonneutral double layer is currently unknown and is why TerDLE will perform a  
436 search (Objective 3). However, if it is ultimately found that the difference in density not resolvable  
437 by the TerDLE instrumentation, that result also will be reported as an upper limit to the electron  
438 and ion density difference (and thus an upper limit of the spatial extent of double layer structure)  
439 during the near-terminator overflights. Hence, a non-detection by TerDLE is still a reportable result.

440         In an updated version of TerDLE, the same science objectives can be achieved by any larger  
441 spacecraft with an ion spectrometer and plasma wave system passing in close proximity to the near-  
442 Moon wake flank. Thus, the science target could be achieved by a large spacecraft proposed under  
443 the NASA SIMPLEX program – which allows for larger bus sizes with expanded funding  
444 envelopes. A larger spacecraft could also include an electron spectrometer. As shown by Halekas  
445 et al. (2005), the electron energy distribution at high energies measured in the wake region provides  
446 a direct measure of the plasma expansion potential. In this application, the wake electron energy

447 distribution systematically shifts to lower energies compared to the energy distribution in the free-  
448 flowing solar wind. The energy shift is a direct measure of the wake potential. Unfortunately,  
449 electron spectrometer systems are sensitive to the negative spacecraft charging expected in  
450 shadowed regions, which would affect (reject) the lower energy electron population. However, the  
451 use of an electron spectrometer as a potential probe as derived by the higher energy electron  
452 population would provide added information on the wake flank.

453 Another possible inclusion to a TerDLE-like concept on a larger bus is a measure of the DC  
454 E-field. Such a sensitive system is currently part of the FIELDS package onboard Parker solar probe  
455 (Bale et al., 2016). Mozer et al. (2020) measured the E-field near the sun at  $< 2$  mV/m (to derive a  
456 Poynting flux,  $EB/\mu_0$ , of  $< 2 \times 10^{-4}$  W/m<sup>2</sup> in a 100 nT B-field). The DC E-field would then provide  
457 a direct measurement of the solar wind convection E-field and possibly the added effect of the  
458 expansion E-field although the latter is near the limit of detection (possibly remains below 1 mV/m,  
459 see Figure 5 of Holmstrom et al. (2012)).

460 Another addition to the payload is a magnetometer. It is well known that diamagnetic  
461 currents flow along the wake flank and these currents can be sensed by the associated perturbation  
462 in the magnetic field (Owen et al., 1996; Halekas et al., 2005). Alfvén wing currents (Zhang et al.,  
463 2016), Mach cone boundary currents, and rarefaction currents (Fatemi et al., 2013) are also  
464 generated by the Moon-solar wind interaction. It would be interesting to know if there are more  
465 complex current structures associated with disturbed particle populations in locations that have non-  
466 neutral expansion fronts. If so, one could search for a correlation between anomalous  
467 magnetometer-sensed currents and plasma wave activity as sensed by the PWS.

468 A key requirement is passing through the near-Moon wake flank at the lowest possible  
469 altitude. As described previously, we expect the expansion front to be a near-perfect discontinuity  
470 just behind the terminator. In regions downstream we then expect the electron cloud and double  
471 layer to form. One possible way to consistently get to very low altitudes ( $< 20$  km) is the use of a  
472 dual-spacecraft tethered satellite system like that described by Collier et al. (2016). While the center  
473 of gravity for the tethered pair can be 50 km, one spacecraft can be located at much lower altitudes—  
474 allowing a sensing of the time-stationary expansion structure just a few kilometers downstream of  
475 its terminator obstruction location on nearly every orbital transit. In fact, in a SIMPLEX call, one  
476 can imagine flying a dual TerDLE, with one cubesat at very low altitudes passing through the wake  
477 region just downstream of the terminator. A ‘tethered TerDLE’ would be an exciting future mission.

478 To summarize, we describe the TerDLE mission to examine the formation region of the  
479 trailing lunar wake that forms in the solar wind plasma flowing anti-sunward from the Moon.  
480 TerDLE is designed to search the near-Moon wake flank region for unusual plasma structures, to  
481 derive solar wind-driven wake variability, and to search for regions where plasma neutrality is lost  
482 (double layers). Immediately downstream of the terminator, it is anticipated that a near-perfect  
483 plasma discontinuity forms, with solar wind on one side and a void on the other. Simulations show  
484 that the first action is to have low mass electrons of larger thermal velocity, move into the void  
485 before the heavier protons – creating a local loss of neutrality. The downstream extent of this non-  
486 neutral region (i.e., double layer) is currently unknown but TerDLE can either define or place limits  
487 on the non-neutral regions extent. While the initial TerDLE concept was proposed as a cubesat for  
488 the Artemis-1 mission, we present other embodiments that include an expanded payload beyond  
489 the IS and PWS. We also describe a future tethered TerDLE mission to consistently obtain low  
490 altitude flybys over the terminator regions where the plasma expansion is initiated.

491

492 **Acknowledgements.** We gratefully acknowledge funding from SSERVI and the LEADER Center  
493 for Space Environments in the preparation of this manuscript.

494

495

## 496 **References**

497

498 Angelopoulos, V. (2011), The ARTEMIS Mission, *Space Sci. Rev.*, 165, 3-25.

499 Bale, S. D. et al., (1997), *Geophys. Res. Lett.*, 24, 1427.

500 Bale, S. D., K. Goetz, P. R. Harvey, et al. (2016), *Space Sci. Rev.*, 204, 49-82.

501 Bonnell, J. W., et al. (2008), *Space Sci Rev*, 141:303-341.

502 Bosqued, J. M. et al. (1996), *Geophys. Res. Lett.*, 23, 1259.

503 Clack, D., J. C. Kasper, A. J. Lazarus, J. T. Steinberg, and W. M. Farrell (2004), *Geophys. Res.*  
504 *Lett.*, 31, Art. No. L06812

505 Clark, P., B. Malphrus, D. Reuter, et al. (2017), Using a compact broadband IR spectrometer to  
506 search for lunar volatiles with a first-generation deep space CubeSat," *Proc. SPIE 9978*,  
507 *CubeSats and NanoSats for Remote Sensing*, 99780C (17 March 2017); doi:

508 10.1117/12.2238332

509 Collier, M. R., R. R. Vondrak, R. P. Hoyt, et al. (2016), *Acta Astronautica*, 128, 464-472.  
510 Collier, M. R., D. Chornay, J. Clemmons, et al. (2015), *ASR*, 56:2097-2105.  
511 Crow, J. E., P. L. Auer, and J. E. Allen (1975), *J. Plasma Phys.*, 14, 65,  
512 doi:10.1017/S0022377800025538.  
513 Ergun R. E., L. Andersson, D. Main, et al. (2004), *J. Geophys. Res.*, 109, A12220.  
514 Fatemi, S., et al. (2013), *GRL*, 40:17-21  
515 Farrell, W. M., et al. (1996) *Geophys. Res. Lett.*, 23, 1271.  
516 Farrell, W. M., M. L. Kaiser, and J. T. Steinberg (1997), *Geophys. Res. Lett.*, 24, 1135.  
517 Farrell, W. M., M. L. Kaiser, J. T. Steinberg, and S. D. Bale (1998), *J. Geophys. Res.*, 103,  
518 23,653, doi:10.1029/97JA03717.  
519 Farrell, W. M., T. J. Stubbs, J. S. Halekas, G. T. Delory, M. R. Collier, R. R. Vondrak, and R. P.  
520 Lin (2008), *Geophys. Res. Lett.*, 35, L05105, doi:10.1029/2007GL032653.  
521 Halekas, J. S., S. D. Bale, D. L. Mitchell, and R. P. Lin (2005), *J. Geophys. Res.*, 110, A07222,  
522 doi:10.1029/2004JA010991.  
523 Halekas, J. S. et al. (2011), *Space Sci. Rev.*, 165, 93, DOI 10.1007/s11214-010-9738-8  
524 Halekas, J. S., A. R. Poppe, G. T. Delory, M. Sarantos, W. M. Farrell, V. Angelopoulos, and J. P.  
525 McFadden (2012), *J. Geophys. Res.*, 117, E06006, doi:10.1029/2012JE004107.  
526 Halekas, J. S., Poppe, A. R., Harada, Y., et al. (2018), *Geophysical Research Letters*, 45, 9450–  
527 9459. [https:// doi.org/10.1029/2018GL079936](https://doi.org/10.1029/2018GL079936)  
528 Halekas, J. S, A. R. Poppe, J. P. McFadden (2014), *JGR-Space Physics*, 119, 5133-5149  
529 Holmstrom, M, S., et al. (2012), *Earth Planets Space*, 64, 237-245  
530 Lue, C., Y. Futaana, S. Barabash, et al., (2011), *Geophys. Res. Lett.*, 38, L03202,  
531 doi:10.1029/2010GL046215.  
532 McFadden, J. p, et al. (2008), *Space Sci. Rev.*, 141:277-302  
533 Mozer, F. S. , O. V. Apapitov, S. D Bale, et al. (2020), *ApJS*, 246:68  
534 Ness, N. F., et al., (1968), *J. Geophys. Res.*, 73, 3421-3440.  
535 Ness, N. F. and K. H. Schatten (1969), *J. Geophys. Res.*, 74, 6425-6438.  
536 Ness, N. F. (1972), *Interaction of the solar wind with the Moon*, in *Solar Terrestrial Physics*  
537 1970, part II, edited by E. R. Dyer, pp. 159– 205, Springer, New York.  
538 Nishino, M. N., M. Fujimoto, Y Saito, et al. (2010), *Geophys. Res. Lett.*, 37, L12106,  
539 doi:10.1029/2010GL043948.

540 Ogilvie, K. W., J. T. Steinberg, R. J. Fitzenreiter, C. J. Owen, A. J. Lazarus, W. M. Farrell, and  
541 R. B. Torbert (1996), *Geophys. Res. Lett.*, 23, 1255, doi:10.1029/96GL01069.

542 Owens, C. J., et al. (1996), *Geophys. Res. Lett.*, 23, 1263.

543 Poppe, A. R., S. Fatemi, J. S. Halekas, M. Holmstrom, and G. T. Delory (2014), *Geophys. Res.*  
544 *Lett.*, 41, doi:10.1002/2014GL060280.

545 Rowland, D. E., M. R. Collier, J. B. Sigwarth, et al., (2011), SPIE, IEEEAC paper #1425.

546 Saito, Y., S. Yokota, T. Tanaka, et al. (2008), *Geophys. Res. Lett.*, 35, L24205,  
547 doi:10.1029/2008GL036077

548 Samir, U., K. H. Wright Jr., and N. H. Stone (1983), *Rev. Geophys.*, 21, 1631,  
549 doi:10.1029/RG021i007p01631.

550 Scherbarth, M, D. Smith, A. Adler, et al. (2009), *Solar Physics and Space Weather*  
551 *Instrumentation III*, Ed. S. Fineschi and J. A. Fennelly, SPIE, 2009,  
552 <http://dx.doi.org/10.1117/12.824898>

553 Schubert G. and B. R. Lichtenstein, *Rev. Geophys. Space Phys.*, 12, 592-626, 1974

554 Spreiter, J. R., March, M. C., and Summers, A. L.(1970), *Cosmic Electrodynamics*, Vol. 1, pp. 5–  
555 50.

556 Tribble, A. C., “The Large-Scale Wake Structure of the Shuttle Orbiter: Plasma Density,  
557 Temperature, and Turbulence,” Ph.D. Dissertation, Dept. of Physics, Univ. of Iowa, Iowa  
558 City, IA, May 1988.

559 Tribble, A. C., Pickett, J. S., D’Angelo, N., and Murphy, G.B., “Plasma- Density, Temperature  
560 and Turbulence in the Wake of the Shuttle Orbiter,” *Planetary and Space Science*, Vol.  
561 37, 1989, pp. 1001–1010.

562 Xu, S., Poppe, A. R., Halekas, J. S., Mitchell, D. L., McFadden, J. P., & Harada, Y. (2019),  
563 *Journal of Geophysical Research: Space Physics*, 124, 3360–3377.

564 Xu, S., et al. (2020), *JGR-Space Physics*, 125:e2020JA028154.

565 Zhang, H., K. K. Khurana, M. G. Kivelson, et al. (2014), *JGR- Space Physics*, 119, 5220–5243.

566 Zhang, H. et al. (2016), *JGR-Space Physics*, 121,10698-10711

567 Zimmerman, M. I., W. M. Farrell, T. J. Stubbs, J. S. Halekas, and T. L. Jackson (2011),  
568 *Geophys. Res. Lett.*, 38, L19202, doi:10.1029/2011GL048880.

569 Zimmerman, M.I., Jackson, T.L., Farrell, W.M., Stubbs, T.J., (2012), *J. Geophys. Res.* 117  
570 E00K03.

- 571 Zimmerman, M.I., Farrell, W.M., Stubbs, T.J., (2013), *Icarus* 226, 992–998.
- 572 Zolotukhin, D. B., K. P. Danials, L Brieda, and M. Keidar (2020), *Phys. Rev., R*, 102, 021203(R)
- 573
- 574
- 575